Hindawi
International Journal of Aerospace Engineering
Volume 2018, Article ID 5061948, 11 pages
https://doi.org/10.1155/2018/5061948

Research Article

Numerical Analysis of the Influences of Geometrical Deviation on Delamination in Composite Laminates around the Countersunk Hole

Xueshu Liu,[1] **Yuxing Yang**,[2] **Li Huang**,[1] **Ping Zhang**,[1] **and Hang Gao**[2]

[1]*School of Automotive Engineering, Dalian University of Technology, Dalian 116024, China*
[2]*School of Mechanical Engineering, Dalian University of Technology, Dalian 116024, China*

Correspondence should be addressed to Xueshu Liu; liuxs@dlut.edu.cn

Received 7 August 2017; Accepted 10 December 2017; Published 14 January 2018

Academic Editor: Ratneshwar Jha

During countersunk hole machining, defects like geometrical deviation of the chamfer angle and delamination are easily introduced into the structure. To investigate the influences of geometrical deviation on delamination propagation around the countersunk hole during assembly, a progressive damage model (PDM) combining cohesive element was proposed and validated. Numerical analyses were then carried out to study delamination propagation behavior under the influences of geometrical parameters including delamination factor, chamfer angle, and location of delamination. The results show that when delamination appears at the transition area of the countersunk hole, the load causing the delamination evolution is much smaller than other cases.

1. Introduction

Carbon fiber reinforced plastic (CFRP) possesses the properties of lightweight and high-specific stiffness and strength, all of which make them suitable for a wide range of high responsibility applications in aircraft structures. Although there are many ways to assemble two different CFRP parts, countersunk fasteners provide aerodynamic benefits compared to protruding head ones and are of particular interest for aircraft skin applications [1]. However, delamination is easily introduced at the neighborhood of the countersunk hole in the process of machining such as drilling, which decreases the stiffness of structure, leads to the destruction of laminated plates in advance and seriously affects the safety of the structure of the aircraft. Studies on the effects of delamination on strength of composite structure have been carried out for many years.

Finite element method (FEM) is widely employed to predict the mechanical behavior of composite structures with delamination by means of the virtual crack closure technique (VCCT) [2–5] and cohesive zone model (CZM) [6–8]. The VCCT is based on the assumption of the energy release rate, an initial defect or crack length, and complex mesh moving technique, while CZM can predict both the onset and the non-self-similar propagation of delamination. In recent years, the cohesive element methods have been used widely which can conveniently and accurately predict the delamination initiation and growth. Turon et al. [9, 10] presented an accurate analytical solution for delamination growth under mixed-mode loading using cohesive elements. The significant effects of buckling and delamination growth for various parameters (delamination size and distribution) in slender composite laminate were investigated with FEM based on a cohesive element [11, 12]. Ataş et al. [13–15] conducted numerical analysis to study the clamping force effects on the delamination onset and growth: pinned and bolted (protruding head bolts) composite laminates. One can expect that the compressive normal stresses (σ_{33}) developed under the washer area due to the initial clamping force could suppress the onset of delamination.

McCarthy et al. [16, 17] carried out an experimental and numerical investigation into the effect of clearance on the

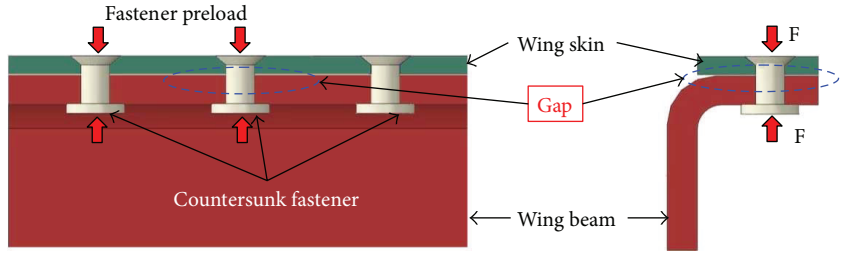

Figure 1: Load condition of wing skin and rib connection structure.

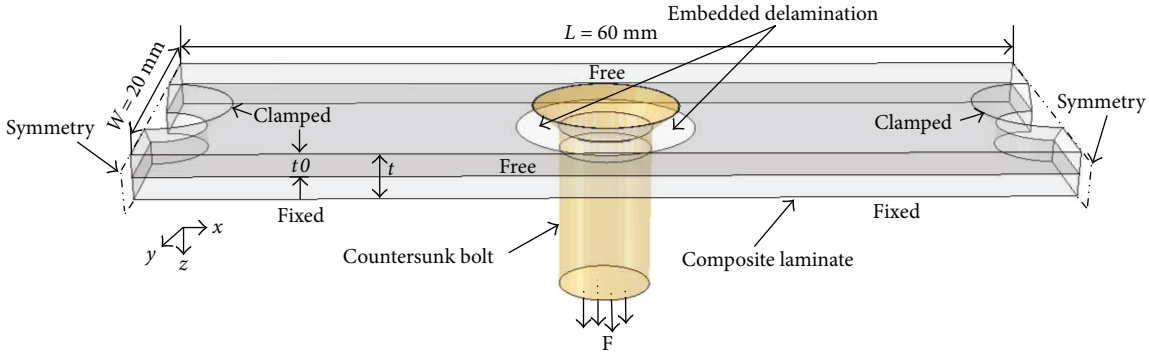

Figure 2: Simplified structural geometry, boundary condition, and applied load.

Table 1: Mechanical properties of IMS194/CYCOM977-2 laminate [20].

E_{11} (GPa)	$E_{22} = E_{33}$ (GPa)	$G_{12} = G_{13}$ (GPa)	G_{23} (GPa)	$\upsilon_{12} = \upsilon_{13}$	υ_{23}
165	8.17	4.27	3.17	0.33	0.48
X_T (MPa)	X_C (MPa)	$Y_T = Z_T$ (MPa)	$Y_C = Z_C$ (MPa)	$S_{12} = S_{13} = S_{23}$ (MPa)	
3150	1450	81.4	270	108	

stiffness and strength of single-bolt, single-lap, and carbon-epoxy joints. Finger-tight and fully torqued conditions were also investigated. Meanwhile, Chishti et al. [18, 19] also performed an experimental and numerical investigation of the effects of bolt torque, clearance, and countersunk height ratio on damage progression and strength of countersunk composite joints. It indicated that the introduction of the countersunk hole roughly halved the bearing stress and caused delamination for some configurations. Increasing the bolt torque was found to increase damage in the countersunk area whilst reducing it close to the shear plane, without affecting the distribution of damage around the hole. Most of them were devoted to investigate that the initial bolt clamping force can suppress the delamination initiation and growth in CFRP under tensile load; few attempts have been made to predict the delamination initiation and propagation in composite laminates during the process of the preloading of bolts, especially when delamination occurs around the countersunk hole.

The aim of this paper is to systematically investigate the factors that affect the growth of delamination around the countersunk hole under the condition of bolt preloading with the progressive damage model (PDM) and cohesive element, which is based on a three-dimensional Hashin-type criterion and bilinear traction-separation law, respectively.

2. Geometry and Materials

Load conditions of wing skin and beam connection structure are shown in Figure 1. Due to the anisotropic properties of CFRP, composite parts are easily prone to warpage during formation. Consequently, there will always be an interfacial gap between assembly components, especially for large parts. Meanwhile, stress concentration is prone to take place at the countersunk located at the skin. In order to facilitate this study, only wing skin is concerned. The configuration of the structure with a countersunk hole and subjected to preloading is shown in Figure 2.

An orthotropic material system of 20 plies of carbon fiber/epoxy (IMS194/CYCOM 977-2) with symmetrical stacking sequence $[45/90/-45/0/90/0/-45/90/45/-45]_S$ is considered in the analysis of the present study [20]. The nominal single-layer thickness of the laminate is 0.15 mm, and its mechanical properties are given in Table 1. The properties of the cohesive layer are listed in Table 2. Bolt is considered as a titanium single solid and the properties are $E = 110$ GPa and $\upsilon = 0.3$.

3. Failure Theory and Finite Element Model

The failure model employed here includes the progressive failure and delamination. The initiation of the failure was

Table 2: The properties of the cohesive layer [21].

G_{IC} (N/mm)	$G_{IIC} = G_{IIIC}$ (N/mm)	${\sigma_n}^0$ (MPa)	${\sigma_s}^0 = {\sigma_t}^0$ (MPa)	K_n (MPa/mm)	$K_s = K_t$ (MPa/mm)
0.478	0.58	12.8	24.2	34,500	3450

Table 3: Failure criteria for unidirectional lamina [22].

Failure mode	Failure criterion
Fiber tensile failure ($\sigma_{11} \geq 0$)	$\left(\frac{\sigma_{11}}{X_T}\right)^2 + \frac{2\tau_{12}^2/G_{12} + 3\alpha\tau_{12}^4}{2S_{12}^2/G_{12} + 3\alpha S_{12}^4} + \frac{2\tau_{13}^2/G_{13} + 3\alpha\tau_{13}^4}{2S_{13}^2/G_{13} + 3\alpha S_{13}^4} = e_{\text{ft}}^2$
Fiber compressive failure ($\sigma_{11} < 0$)	$\left(\frac{\sigma_{11}}{X_C}\right)^2 = e_{\text{fc}}^2$
Fiber matrix shear-out ($\sigma_{11} < 0$)	$\left(\frac{\sigma_{11}}{X_C}\right)^2 + \frac{2\tau_{12}^2/G_{12} + 3\alpha\tau_{12}^4}{2S_{12}^2/G_{12} + 3\alpha S_{12}^4} + \frac{2\tau_{13}^2/G_{13} + 3\alpha\tau_{13}^4}{2S_{13}^2/G_{13} + 3\alpha S_{13}^4} = e_{\text{fms}}^2$
In-plane matrix cracking ($\sigma_{22} \geq 0$)	$\left(\frac{\sigma_{22}}{Y_T}\right)^2 + \frac{2\tau_{12}^2/G_{12} + 3\alpha\tau_{12}^4}{2S_{12}^2/G_{12} + 3\alpha S_{12}^4} + \left(\frac{\tau_{23}}{S_{23}}\right)^2 = e_{\text{imt}}^2$
In-plane matrix crushing ($\sigma_{22} < 0$)	$\left(\frac{\sigma_{22}}{Y_C}\right)^2 + \frac{2\tau_{12}^2/G_{12} + 3\alpha\tau_{12}^4}{2S_{12}^2/G_{12} + 3\alpha S_{12}^4} + \left(\frac{\tau_{23}}{S_{23}}\right)^2 = e_{\text{imc}}^2$
Out-of-plane matrix cracking ($\sigma_{33} \geq 0$)	$\left(\frac{\sigma_{33}}{Z_T}\right)^2 + \frac{2\tau_{13}^2/G_{13} + 3\alpha\tau_{13}^4}{2S_{13}^2/G_{12} + 3\alpha S_{13}^4} + \left(\frac{\tau_{23}}{S_{23}}\right)^2 = e_{\text{omt}}^2$
Out-of-plane matrix crushing ($\sigma_{33} < 0$)	$\left(\frac{\sigma_{33}}{Z_C}\right)^2 + \frac{2\tau_{13}^2/G_{13} + 3\alpha\tau_{13}^4}{2S_{13}^2/G_{12} + 3\alpha S_{13}^4} + \left(\frac{\tau_{23}}{S_{23}}\right)^2 = e_{\text{omc}}^2$

determined by three-dimensional Hashin-type criteria and the modified Tserpes' material degradation model [22, 23]. The delamination, on the other hand, was modeled using cohesive elements.

3.1. Progressive Failure Model. Generally, the progressive failure analysis of the composite laminate material consists of two major steps [24]. The first step is to choose the appropriate failure criteria to determine which kind of failure mode will occur. Although many failure criteria had been reported so far, the Hashin-type criteria have been widely used because it has the ability to distinguish seven failure models of composite laminate and suits for three-dimensional conditions as present in this literature. Therefore, the 3D Hashin-type failure criteria are adopted for the failure predictions of composite materials, which is shown in Table 3, where σ_{ij} ($i,j = 1, 2, 3$) are the scalar components of the stress tensor, and S_{ij} ($i,j = 1, 2, 3$) are the material strengths in longitude, transverse, and through-the-thickness directions of lamina, respectively. The superscripts T and C denote tension and compression, respectively, and α is a constant parameter related to the shear nonlinear behavior, which is determined experimentally. In any element, when the criterion $e > 1$ is satisfied, the element fails by the associated failure.

The second step is to choose the suitable material degradation rules for a reduction in stiffness of the composite material after the occurrence of a certain type of failure. The commonly used degradation methods are the total discount method, the limit discount method, and the residual property method. Since Tserpes' material degradation model contains seven failure modes and corresponds to the 3D Hashin-type failure criteria, on the basis of the modified Tserpes' material degradation model, the limit discount method of the unidirectional lamina is applied in this research, and the degradation rules are shown in Table 4. The failure criteria and the degradation rules of composite materials are implemented through the ABAQUS user subroutine UMAT.

The flow chart of the UMAT subroutine is given in Figure 3. The simulation procedure stops as soon as either the displacement load is reached or the simulation fails to converge prematurely. In this study, the equal strain formats of the failure criteria are used for simplicity. In addition, in order to improve convergence, the viscous regularization technique of the damage variables is implemented with discretized form. Since the subroutine is not the focus of this study, for details, please refer to [25].

3.2. Delamination. It has been proved that the bilinear traction-separation law can perfectly represent delamination initiation and propagation. So, in this study, the interface damage is modelled using the traction-separation law, which is commonly used to describe the delamination of the composite. Interfacial failure or delamination is assumed to initiate once the following quadratic interactive criterion is satisfied:

$$\sqrt{\left(\frac{\langle t_n \rangle}{\sigma_n^c}\right)^2 + \left(\frac{t_s}{\sigma_s^c}\right)^2 + \left(\frac{t_t}{\sigma_t^c}\right)^2} = 1, \quad (1)$$

where the symbol $\langle\ \rangle$ represents the Macaulay bracket operator. t_n, t_s, and t_t are the normal stress and the two shear

Table 4: Material degradation model [23].

Failure mode	Material properties' degradation factors								
	E_{11}	E_{22}	E_{33}	G_{12}	G_{13}	G_{23}	υ_{12}	υ_{13}	υ_{23}
Fiber tensile failure	0.009	—	—	—	—	—	—	—	—
Fiber compressive failure	0.044	—	—	—	—	—	—	—	—
In-plane matrix cracking	—	0.1	—	0.1	—	0.1	—	—	—
In-plane matrix crushing	—	0.2	—	0.2	—	0.2	—	—	—
Out-of-plane matrix cracking	—	—	0	—	0	0	—	0	—
Out-of-plane matrix crushing	—	—	0	—	0	0	—	0	—
Fiber matrix shear-out	—	—	—	0.08	0.08	0.13	0.08	0.08	0.13

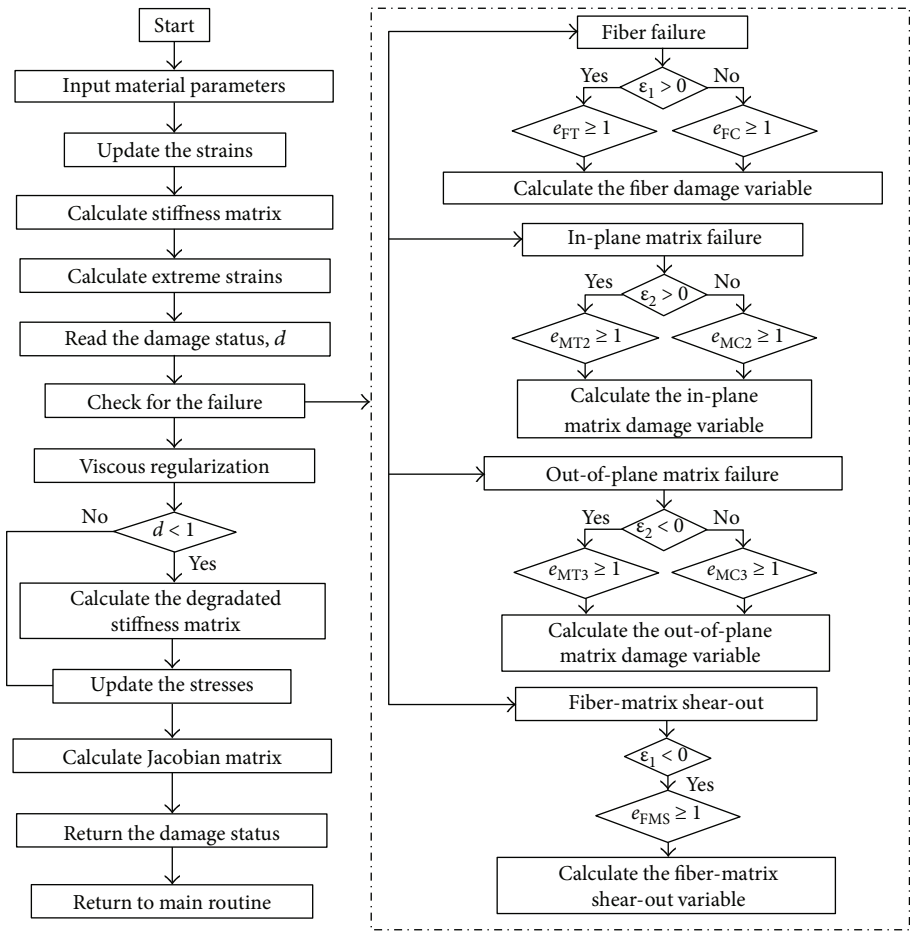

Figure 3: Flowchart of the UMAT subroutine.

stresses on the interface, and σ_n^c, σ_s^c, and σ_t^c are the normal strength and the two shear strengths of the interface.

Under mixed-mode loading, the bilinear softening constitutive law was used for delamination propagation and the mixed-mode fracture energy criterion developed by Benzeggagh and Kenane [26] was used here (B-K criterion). If mode III occurs, the criterion can be given by

$$G_{IC} + (G_{IIC} - G_{IC}) \left\{ \frac{G_{II} + G_{III}}{G_I + G_{II} + G_{III}} \right\}^{\eta} = G_C, \quad (2)$$

where G_I, G_{II}, and G_{III} are the modes I, II, and III strain energy release rates. G_{IC} and G_{IIC} are the critical strain energy release rate (fracture toughness) in modes I and II. η is a material parameter, which can be obtained by the mix-mode bending test and $\eta = 2.0$ in this study [27].

3.3. Finite Element Model. The composite laminate was modeled by the 8-node reduced integration solid elements (C3D8R). Since the delamination mainly occurs at the interfaces between composite plies, the interface between

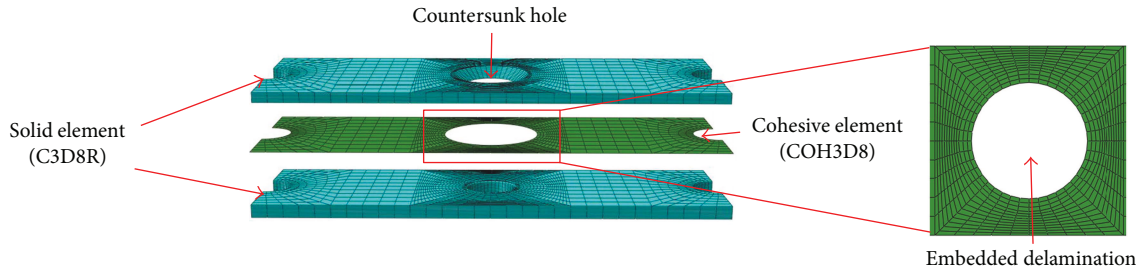

Figure 4: The structure of the composite layer and interface.

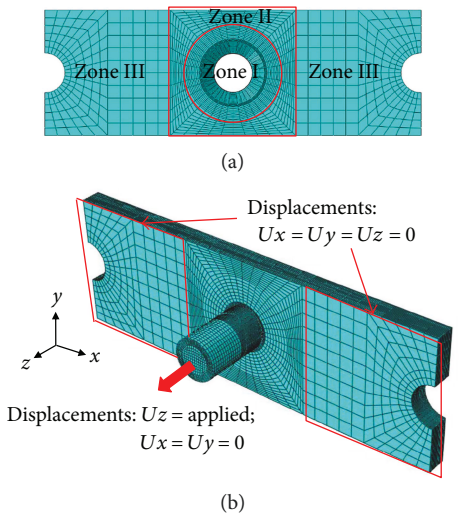

Figure 5: (a) Adopted finite element discretization including delamination area (zone I) and propagation area (zone II and zone III). (b) The boundary conditions of the composite laminate.

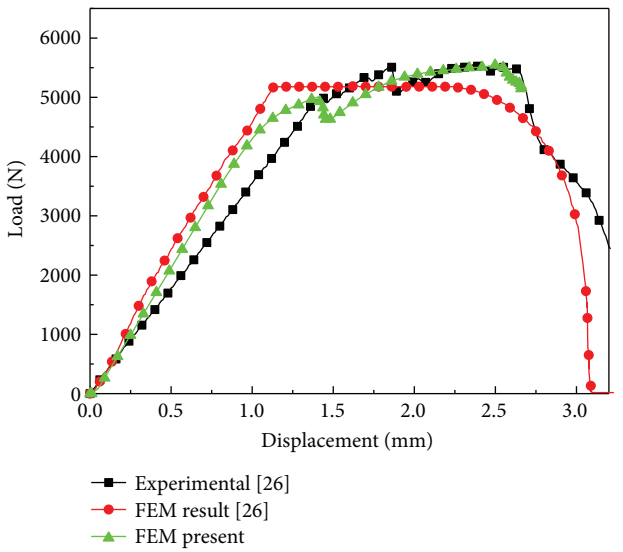

Figure 6: Load-displacement curves. Numerical predictions and experimental results.

two sublaminates has been modeled by the zero-thickness 8-node 3D cohesive element (COH3D8) to predict delamination propagation.

The structure of the composite layer and interface including the embedded delamination defect around the countersunk hole is illustrated in Figure 4. The cohesive layer was created by the offset method and inserted into two laminate plies [20]. In order to assure that the results are not dependent upon the element's size, the mesh refinement process is necessary. For the details, please refer to [28]. After refinement, the composite plate was modelled with 26,140 elements and the cohesive layer with 940 elements, and 20,916 elements were used to model the bolt. The finite element mesh of the specimen is shown in Figure 4(a). The cohesive element has been positioned in the area (Figure 5(a), zones II and III) around the embedded delamination defect (Figure 5(a), zone I) to predict the delamination evolution. The boundary conditions are shown in Figure 5(b). Surface-to-surface contact element has been placed in the delamination zone to avoid overlaps between elements. Due to large displacements and composite material behavior, the nonlinear stress calculation of the problems presented here was performed using the ABAQUS/Standard code.

4. Results and Discussion

4.1. Model Validation. In order to verify the effectiveness of the proposed method of combining the abovementioned progressive damage method and cohesive model, the finite element model was established according to the geometry and material parameters in the literature [29]. The countersunk head (CS) specimens used was the HL523 pin with HL97 collar. The CFRP material used was CYCOM970 PWC T300 3 K ST, a plain weave epoxy prepreg with ply thickness of 0.22 mm. A symmetric, nominally quasi-isotropic lay-up was used in all specimens. A test rig was designed to determine the pullout loads of fasteners in composite laminates under a quasi-static tensile load condition. The obtained numerical results were compared with the experimental data and numerical prediction from literature [29], as shown in Figure 6. An excellent agreement between numerical prediction and experimental data was found in both stiffness and bearing strength. The proposed method predicted the initial subcritical failure load of 5005 N, similar to the experimental result of 5000 N, with an error less than 0.1%, and the error of bearing failure load obtained from numerical result of 5561 N and experimental data of 5545 N was only 0.3%. Moreover, the present model can reproduce

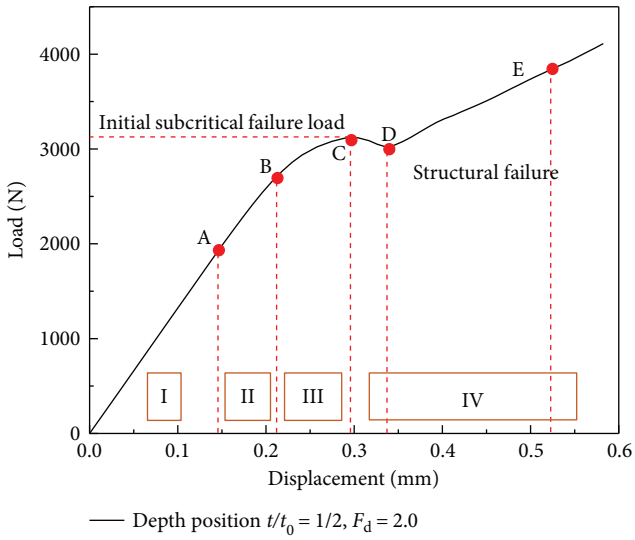

FIGURE 7: Typical load-displacement curve of a composite laminate with delamination defect.

the nonlinearity of the load-displacement curve and the progressive damage of the structure.

4.2. Delamination Propagation around the Countersunk Hole. As mentioned above, the structure of the study under the bolt preload can be simulated by applying the pull-through load. When there is an embedded delamination defect around the countersunk hole in composite laminate, the defect is easy to propagate under the condition of large bolt preloading. Three typical processes of delamination propagation are damage initiation, damage evolution, and structural failure. Figure 7 shows a typical load/displacement curve of a laminate with circular shape delamination defect ($R = 6$ mm), which has been examined by the similar experimental results in the literature [30]. Those processes can be decomposed into four main steps:

(i) Step I: no damage, linear elastic behavior

(ii) Step II: delamination initiation (see Figure 8(a))

(iii) Step III: delamination propagation (see Figures 8(b) and 8(c))

(iv) Step IV: stiffness decrease, with first audible cracks: structural failure (see Figures 8(d) and 8(e))

4.3. Effects of Geometrical Deviation on the Delamination

4.3.1. Effect of the Delamination Factor. The delamination factor has been widely used to characterize the level of damage on drilling the countersunk hole, as shown in Figure 9 The delamination factor (F_d) can be calculated from the ratio of the maximum diameter (D_{max}) of the delamination zone to the drill diameter (D_0), as given in [30]

$$F_d = \frac{D_{max}}{D_0}. \quad (3)$$

In order to expatiate on the delamination size factor, four kinds of the composite laminates with different F_d (1.0, 1.5, 2.0, and 2.5) were investigated, which were under the condition of the same countersunk angle (100°) and through-the-thickness position ($t/t_0 = 1/2$), as shown in Figure 9(a). Figure 10 shows the variation of bearing load as a function of F_d for the case of through-the-thickness position $t_0/t = 1/2$. The initial subcritical failure load decreases as F_d increases from 1.0 to 2.5. Meanwhile, the increase of F_d also leads to the structural stiffness decreasing. When F_d is increased up to 2.5 (i.e., $D_{max} = 15$ mm), the stiffness of structure directly declined by 17.75% compared with that of the no defect one. It is easy to understand that the extremely large delamination area results in a decrease in the plate resistance against the bearing behavior. Thus, new damage is produced at a far lower bolt preloading level.

Moreover, the load causing delamination evolution decreases with the increase of F_d, which can be seen from Figure 11. When F_d is increased up to 2.5, the load declined obviously by 10.26% compared with that of the none embedded one and was very close to the initial subcritical failure load. As explained in the literature [31], the delamination occurs abruptly at the beginning of the test when the load is relatively low (i.e., the lower initial subcritical failure load).

The shapes of the initial damage vary a lot with the change of F_d (Figures 11(a)–11(d)). When there is no embedded delamination defect or in small size, the area of the initial damage is larger (Figures 11(a) and 11(b)). In addition, the damage evolves from the nearby hole to the hole boundary for the no embedded defect case, while the propagation path is opposite for the other case. This is due to the appearance of the embedded delamination defect and its size affects the propagation path.

4.3.2. Effect of the Chamfer Angle. As explained before, we investigated the rib- and wing skin-connecting structure, using the countersunk bolt joints, and the wing skin needs to be drilled by countersunk holes. In the process of drilling, however, it is not only possible to introduce the delamination defect around the countersunk hole but also the deviation of chamfer angle, as shown in Figure 12. As we only focus on the standard 100° countersunk-head fasteners in this study, which were made of titanium alloy (Ti-6Al-4 V), so the countersunk angle θ_c of the composite laminate is $100° \pm 2°$ (i.e., $\theta_c = 98°$, 99°, 100°, 101°, and 102°).

Figures 13 and 14 show the effects of the countersunk in the laminate plate on the delamination evolution and the initial subcritical failure load under different delamination factors. When the countersunk angle of the laminate is small ($\theta_c < 100°$, Figure 12(a)), the load causing delamination evolution and bearing capacity increase by 59 N and 58 N, respectively, with the reduction of the countersunk angle per 1°. The reason for this phenomenon is that the bolt-head will firstly contact with the upper surface of the plate and then the transition area due to the fact that the bolt angle is larger than that of the countersunk. Thus, the bolt will bear the upper surface of the plate and then press the transition area (see Figure 12(a)), which can suppress the onset and propagation of delamination. As shown in Figure 12(b),

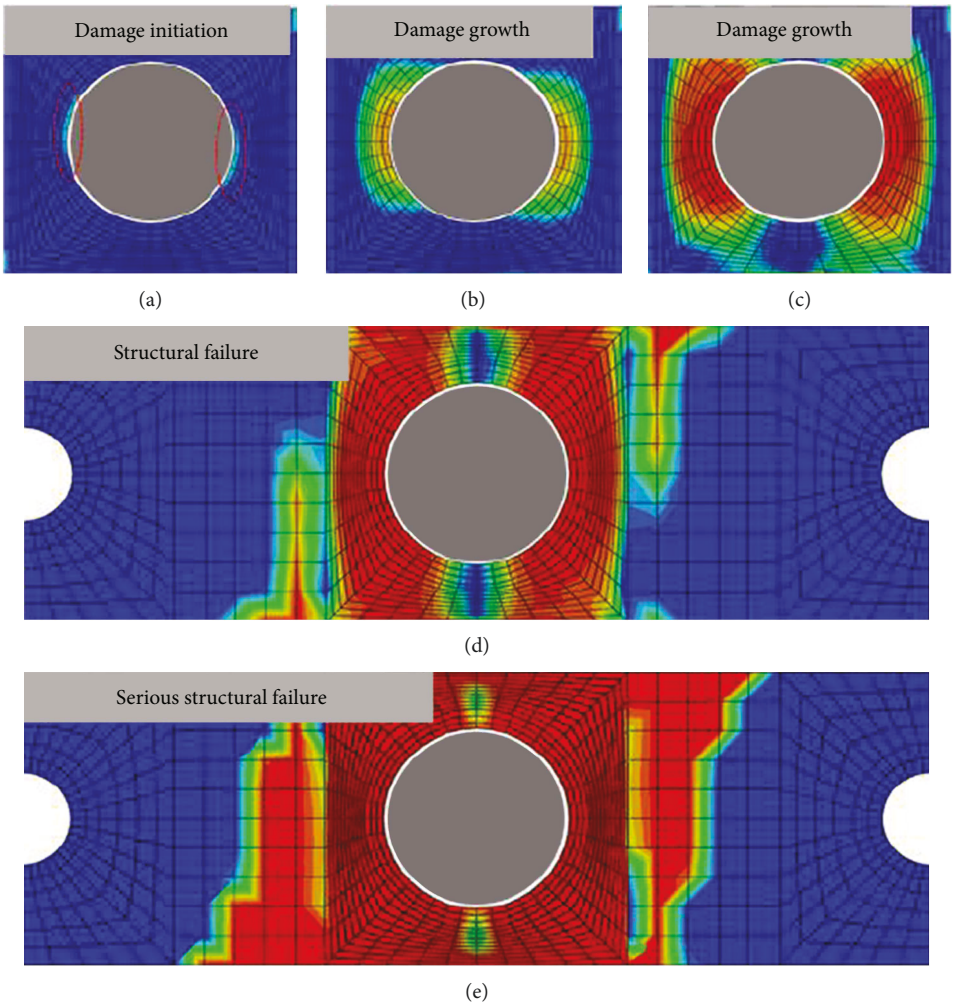

Figure 8: Process of delamination propagation: damage initiation, damage evolution, and structural failure.

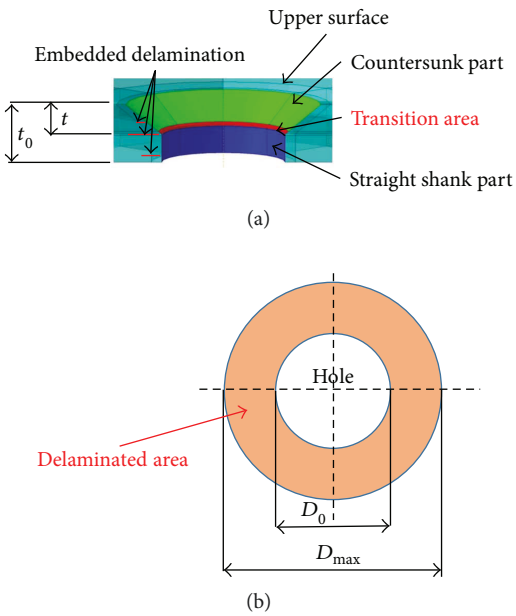

Figure 9: (a) A schematic diagram of the countersunk hole. (b) Uniform delaminated area around the hole.

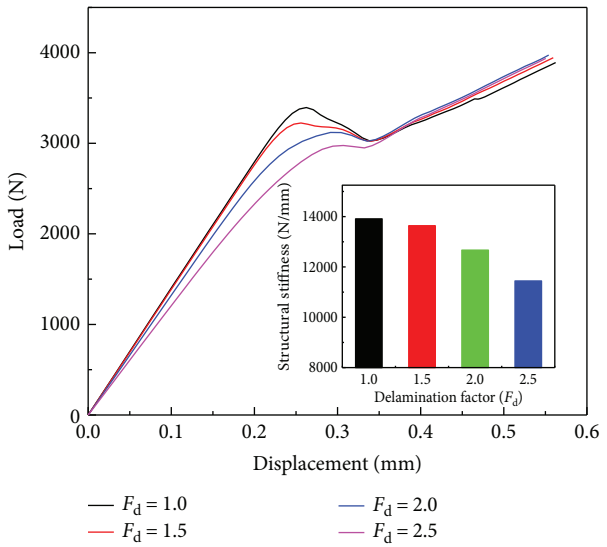

Figure 10: Effect of delamination scale on bearing capacity and structural stiffness.

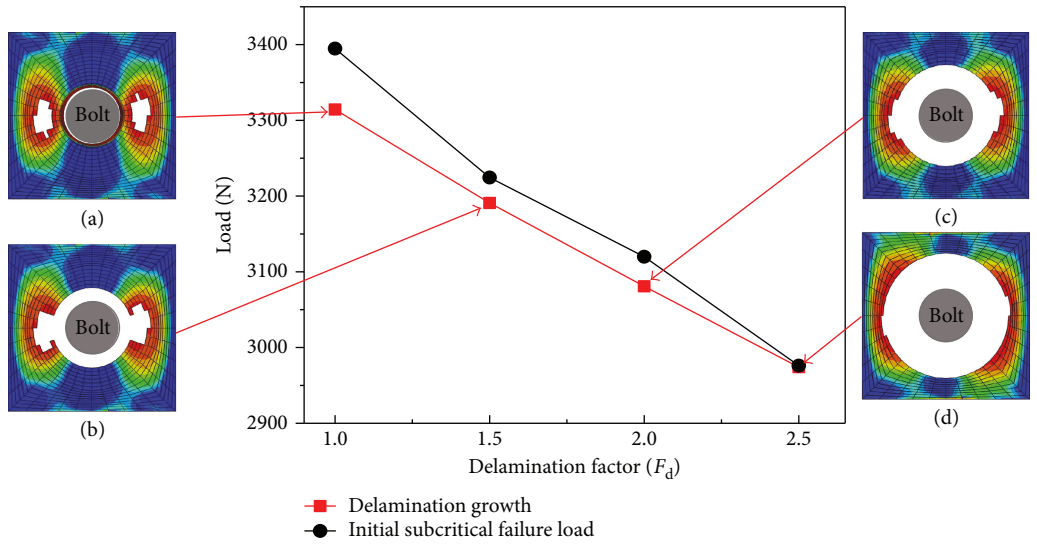

Figure 11: Effect of F_d on the delamination initiation, initial subcritical failure load, and the propagation of delaminated area: (a) $F_d = 1.0$, (b) $F_d = 1.5$, (c) $F_d = 2.0$, and (d) $F_d = 2.5$.

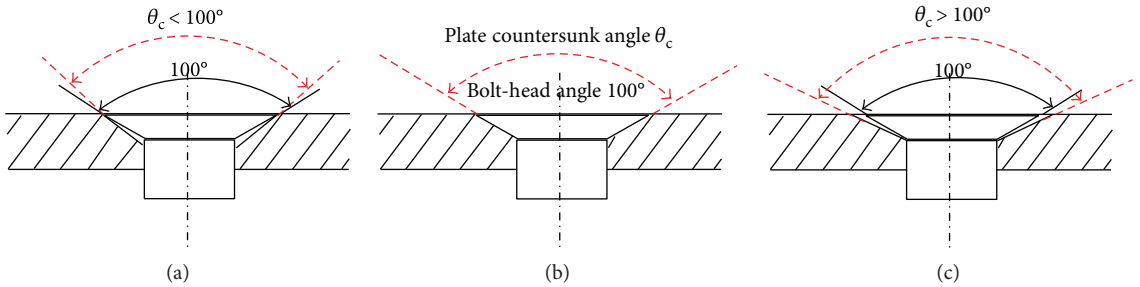

Figure 12: Difference of the drilling countersunk-head angle θ_c in the laminated plate at the bolt-head angle 100°: (a) small $\theta_c < 100°$, (b) standard $\theta_c = 100°$, and (c) large $\theta_c > 100°$.

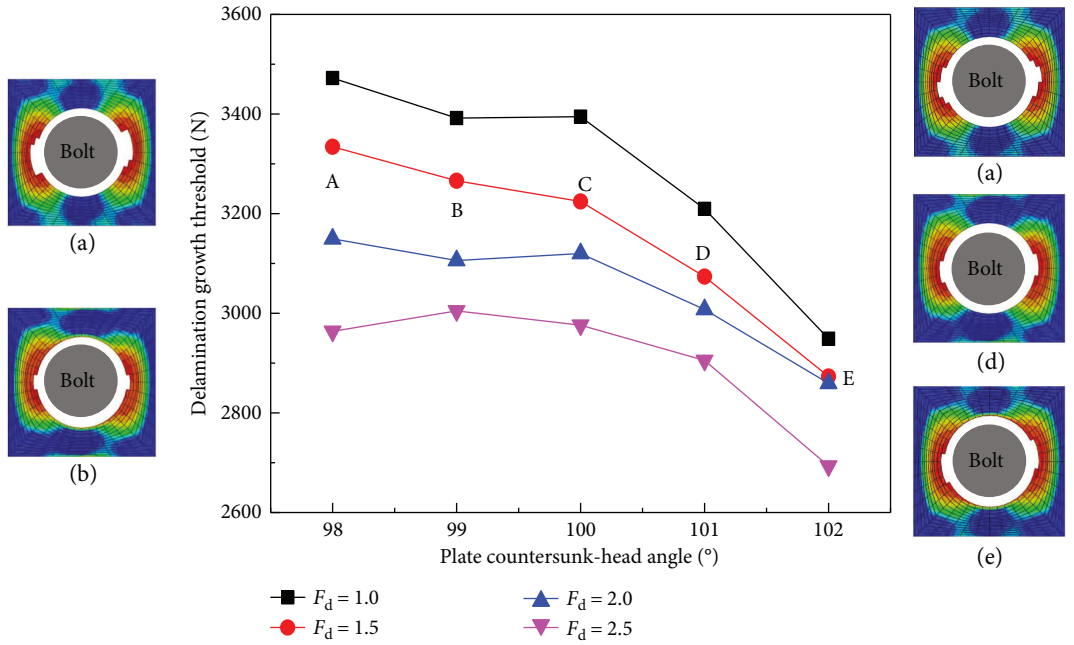

Figure 13: Influence of deviation of the countersunk on the delamination evolution under different delamination factors.

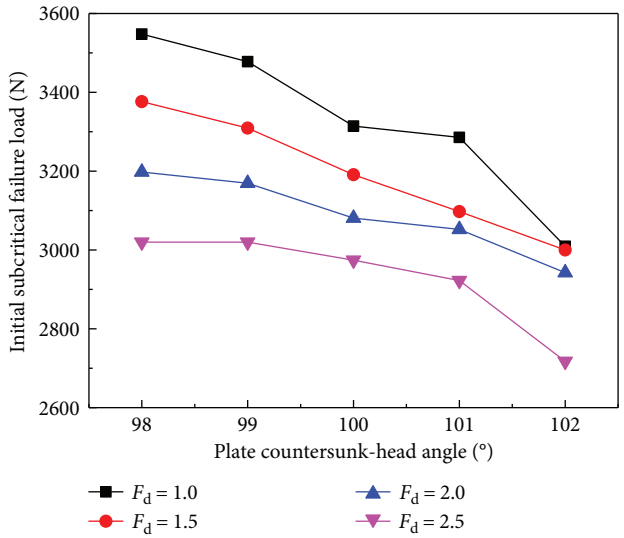

Figure 14: Influence of deviation of the countersunk on the initial subcritical failure load under different delamination factors.

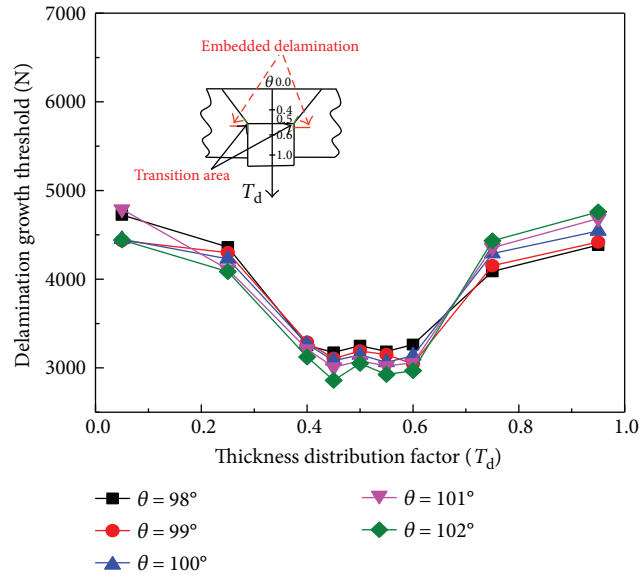

Figure 15: Effect of T_d on delamination evolution threshold under different countersunk-head angles.

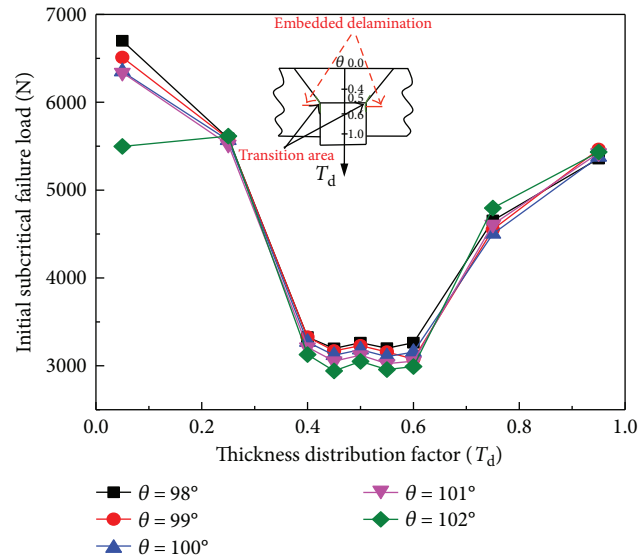

Figure 16: Effect of T_d on the initial subcritical failure load under different countersunk-head angles.

when the countersunk angle of the composite plate is large ($\theta_c > 100^\circ$), with per 1° increasing, the load causing delamination evolution declines by 129 N, and the bearing capacity decreases by 117 N. As the countersunk hole of the plate is larger than that of the countersunk bolt, the bolt directly bears the transition area of the countersunk, leading to delamination evolution which occurs at the transition zone.

No matter how different the countersunk angle is, the damage occurs at almost the same location on condition that the embedded delamination defect locates at the same through-the-thickness position (Figures 13(a)–13(e)), which implies that the countersunk angle only has influence on the load causing delamination evolution.

4.3.3. Effect of the Delamination Location. In order to describe the position of the embedded delamination defect through the thickness of the plate, the thickness distribution factor (T_d) is defined as the ratio of the distance (t) from the embedded delamination defect to the upper plate surface to the plate thickness (t_0), as shown in Figure 9(a). When the plates are drilled, it is easy to introduce delamination defects into the transition area of the countersunk holes. Therefore, we only focus on the delamination appearing in the transition region.

Figures 15 and 16 show the variation of delamination evolution thresholds and the initial subcritical failure loads as a series of T_d, namely, $T_d = 0.05$, 0.25, 0.40, 0.45, 0.50, 0.55, 0.60, 0.75, and 0.95, respectively, under the condition of different countersunk angles in the laminated plate. It is easy to notice that the delamination evolution thresholds and the initial subcritical failure loads are influenced by T_d remarkably. When there is an embedded delamination at the transition area of the countersunk hole, the delamination evolution threshold decreases to 67% with that of the other cases. Meanwhile, the initial subcritical failure load declines to 42%. The appearance of the delamination in the transition area leads to lower delamination evolution threshold and initial subcritical failure load and is the most dangerous case, which should be avoided during hole drilling.

Meanwhile, it was found that the dangerous transition area is within upper and lower 10% plate thickness from the junction of the countersunk part and straight shank part. The reason is that in the process of preloading of the bolt, the stress concentrates in the transition zone of the countersunk hole, and delamination in this region is easier to propagate. The parameter of T_d plays a predominant role in determining the delamination evolution behavior and the composite plate with the delamination defect in the transition zone of the countersunk which has an extremely low-structure bearing capacity.

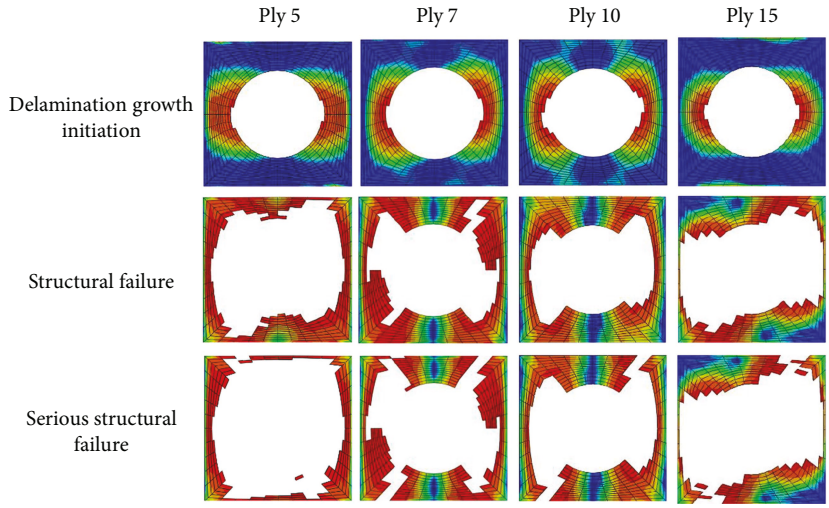

Figure 17: Delamination evolution with $F_d = 2.0$ and different T_d.

Figure 17 shows the propagation of the delaminated area with different T_d (1/4, 7/20, 1/2, and 3/4) under the condition of $F_d = 2.0$ and $\theta_c = 100^\circ$. As mentioned above, the appearance of delamination in the transition area leads to a lower delamination evolution threshold and initial subcritical failure load. Simultaneously, it can be seen that the damage regions change a lot when T_d varies.

5. Conclusions

In this paper, the delamination initiation and evolution in composite laminates are investigated by using FEM based on PDM and the cohesive element method. When there is an embedded delamination around the countersunk hole in composite laminate, the critical load causing delamination growth is much smaller than other cases, and the defect is easy to propagate under the process of larger bolt preloading. The size and through-the-thickness position of delamination and plate countersunk angle have significant effects upon the delamination initiation and propagation behavior of composite laminates.

Generally, as the delamination factor F_d increases the load causing delamination evolution decreases. Meanwhile, the increase of F_d also leads to the structural stiffness decreasing. With the increase of θ_c, the delamination evolution threshold and the initial subcritical failure load decrease. In terms of the position of delamination, when there is an embedded delamination at the transition area of the countersunk hole, the critical load causing delamination evolution decreases to 67% of other cases; however, the initial subcritical failure load declines to 42%. Simultaneously, it was found that the dangerous region of the transition area is within upper and lower 10% plate thickness from the junction of the countersunk part and the straight shank part.

The shape of damage is affected by the delamination factor F_d and delamination position T_d, instead of the plate countersunk angle θ_c. As the embedded delamination in the countersunk part is away from the transition area, only a larger bolt preloading can result in delamination evolution. Meanwhile, the width of the propagation zone is ever decreasing as the embedded delamination through-the-thickness positions closer to the transition area.

Conflicts of Interest

The authors declare that they have no conflicts of interest.

Acknowledgments

This work was supported by the National Natural Science Foundation of China (Grant nos. 51375068 and 51475073), the Major State Basic Research Development Program (Grant no. 2014CB046504), the Fundamental Research Funds for the Central Universities (Grant no. DUT17JC19), and the Scientific Research Foundation for the Returned Overseas Chinese Scholars, State Education Ministry. The authors would like to acknowledge the above financial supports.

References

[1] B. Egan, C. T. McCarthy, M. A. McCarthy, P. J. Gray, and R. M. Frizzell, "Modelling a single-bolt countersunk composite joint using implicit and explicit finite element analysis," *Computational Materials Science.*, vol. 64, pp. 203–208, 2012.

[2] R. Krueger, "Virtual crack closure technique: history, approach, and applications," *Applied Mechanics Reviews*, vol. 57, no. 2, pp. 109–143, 2004.

[3] A. C. Orifici and R. Krueger, "Benchmark assessment of automated delamination propagation capabilities in finite element codes for static loading," *Finite Elements in Analysis and Design*, vol. 54, pp. 28–36, 2012.

[4] A. Riccio, A. Raimondo, F. D. Caprio, and F. Scaramuzzino, "Delaminations buckling and growth phenomena in stiffened composite panels under compression. Part II: a numerical study," *Journal of Composite Materials*, vol. 48, no. 23, pp. 2857–2870, 2014.

[5] M. Marjanović, G. Meschke, and D. Vuksanović, "A finite element model for propagating delamination in laminated composite plates based on the virtual crack closure method," *Composite Structures*, vol. 150, pp. 8–19, 2016.

[6] P. P. Camanho, C. G. Davila, and M. F. De Moura, "Numerical simulation of mixed-mode progressive delamination in composite materials," *Journal of Composite Materials*, vol. 37, no. 16, pp. 1415–1438, 2003.

[7] Q. Yang and B. Cox, "Cohesive models for damage evolution in laminated composites," *International Journal of Fracture*, vol. 133, no. 2, pp. 107–137, 2005.

[8] Q. Ye and P. Chen, "Prediction of the cohesive strength for numerically simulating composite delamination via CZM-based FEM," *Composites Part B: Engineering*, vol. 42, no. 5, pp. 1076–1083, 2011.

[9] A. Turon, P. P. Camanho, J. Costa, and C. G. Dávila, "A damage model for the simulation of delamination in advanced composites under variable-mode loading," *Mechanics of Materials*, vol. 38, no. 11, pp. 1072–1089, 2006.

[10] A. Turon, P. P. Camanho, J. Costa, and J. Renart, "Accurate simulation of delamination growth under mixed-mode loading using cohesive elements: definition of interlaminar strengths and elastic stiffness," *Composite Structures*, vol. 92, no. 8, pp. 1857–1864, 2010.

[11] R. G. Wang, L. Zhang, J. Zhang, W. B. Liu, and X. D. He, "Numerical analysis of delamination buckling and growth in slender laminated composite using cohesive element method," *Computational Materials Science*, vol. 50, no. 1, pp. 20–31, 2010.

[12] R. G. Wang, L. Zhang, W. B. Liu et al., "Numerical analysis of delamination behavior in laminated composite with double delaminations embedded in different depth positions," *Polymers & Polymer Composites*, vol. 19, no. 2/3, p. 213, 2011.

[13] A. Ataş, G. F. Mohamed, and C. Soutis, "Effect of clamping force on the delamination onset and growth in bolted composite laminates," *Composite Structures*, vol. 94, no. 2, pp. 548–552, 2012.

[14] A. Ataş and C. Soutis, "Strength prediction of bolted joints in CFRP composite laminates using cohesive zone elements," *Composites Part B: Engineering*, vol. 58, pp. 25–34, 2014.

[15] A. Ataş and C. Soutis, "Application of cohesive zone elements in damage analysis of composites: strength prediction of a single-bolted joint in CFRP laminates," *International Journal of Non-Linear Mechanics*, vol. 66, pp. 96–104, 2014.

[16] M. A. McCarthy, V. P. Lawlor, P. C. O'Donnell, K. Harris, P. Kelly, and J. P. Cunningham, "Measurement of bolt preload in torqued composite joints," *Strain*, vol. 41, no. 3, pp. 109–112, 2005.

[17] B. Egan, C. T. McCarthy, M. A. McCarthy, and R. M. Frizzell, "Stress analysis of single-bolt, single-lap, countersunk composite joints with variable bolt-hole clearance," *Composite Structures*, vol. 94, no. 3, pp. 1038–1051, 2012.

[18] M. Chishti, C. H. Wang, R. S. Thomson, and A. C. Orifici, "Numerical analysis of damage progression and strength of countersunk composite joints," *Composite Structures*, vol. 94, no. 2, pp. 643–653, 2012.

[19] M. Chishti, C. H. Wang, R. S. Thomson, and A. C. Orifici, "Experimental investigation of damage progression and strength of countersunk composite joints," *Composite Structures*, vol. 94, no. 3, pp. 865–873, 2012.

[20] X. Liu, L. Huang, M. Xu, M. Xu, and Z. Zhang, "Influence of different modeling strategies for CFRP on finite element simulation results," *MATEC Web of Conferences*, vol. 67, article 06083, 2016.

[21] Cytec, *CYCOM 977-2 Epoxy Resin System. Technical Data Sheet*, 2012, http://www.cytec.com.

[22] Á. Olmedo and C. Santiuste, "On the prediction of bolted single-lap composite joints," *Composite Structures*, vol. 94, no. 6, pp. 2110–2117, 2012.

[23] J. Zhang, L. Zhou, Y. Chen, L. Zhao, and B. Fei, "A micromechanics-based degradation model for composite progressive damage analysis," *Journal of Composite Materials*, vol. 50, no. 16, pp. 2271–2287, 2016.

[24] G. Alfano and M. A. Crisfield, "Finite element interface models for the delamination analysis of laminated composites: mechanical and computational issues," *International Journal for Numerical Methods in Engineering*, vol. 50, no. 7, pp. 1701–1736, 2001.

[25] Y. X. Yang, X. S. Liu, Y. Q. Wang, H. Gao, R. P. Li, and Y. J. Bao, "A progressive damage model for predicting damage evolution of laminated composites subjected to three-point bending," *Composites Science and Technology*, vol. 151, pp. 85–93, 2017.

[26] M. L. Benzeggagh and M. Kenane, "Measurement of mixed-mode delamination fracture toughness of unidirectional glass/epoxy composites with mixed-mode bending apparatus," *Composites Science and Technology*, vol. 56, no. 4, pp. 439–449, 1996.

[27] W. R. Gong, J. L. Chen, and E. A. Patterson, "Buckling and delamination growth behaviour of delaminated composite panels subject to four-point bending," *Composite Structures*, vol. 138, pp. 122–133, 2016.

[28] L. B. Zhao, Y. Gong, J. Y. Zhang, Y. Chen, and B. J. Land Fei, "Simulation of delamination growth in multidirectional laminates under mode I and mixed mode I/II loadings using cohesive elements," *Composite Structures*, vol. 116, pp. 509–522, 2014.

[29] A. J. Gunnion, H. Körber, D. J. Elder, and R. S. Thomson, "Development of fastener models for impact simulation of composite structures," in *25th Congress of the International Council of Aeronautical Sciences ICAS*, Hamburg, Germany, 2006.

[30] J. P. Davim, J. C. Rubio, and A. M. Abrao, "A novel approach based on digital image analysis to evaluate the delamination factor after drilling composite laminates," *Composites Science and Technology*, vol. 67, no. 9, pp. 1939–1945, 2007.

[31] G. Catalanotti, P. P. Camanho, P. Ghys, and A. T. Marques, "Experimental and numerical study of fastener pull-through failure in GFRP laminates," *Composite Structures*, vol. 94, no. 1, pp. 239–245, 2011.